Full Length Article

Catalytic performance of cobalt supported onto APTES functionalized TiO_2 for Fischer-Tropsch reaction

Francisco Platero, Alfonso Caballero, Gerardo Colón [*]

Instituto de Ciencia de Materiales de Sevilla. Centro Mixto, Universidad de Sevilla-CSIC, Américo Vespucio s/n., 41092 Sevilla, Spain

ARTICLE INFO

ABSTRACT

Cobalt supported TiO_2 catalysts have been prepared by wet-impregnation and by immobilization over APTES (3-aminopropyl triethoxysilane) grafted TiO_2. Impregnated system showed better catalytic performance after reduction at 260 °C but significant deactivation is observed. On the contrary, functionalized catalyst showed better catalytic performance after reduction at 400 °C with notable stability. We have stated from CO-DRIFT *operando* analysis that impregnated system is strongly affected by negative SMSI (strong metal-support interaction) upon reduction at higher temperature. While immobilization on APTES hinders the loss of metal active sites. The study of spent catalysts denotes that Co is redispersed in the impregnated catalyst while functionalized trends to form agglomerates.

1. Introduction

During last decades, energy-dense fossil fuels has been the basis of the energy scheme of the actual society. Growing concerns about the limited fossil fuel supply as well as increasing serious environmental problems has glowed the global interest in green fuels production technologies [1]. Within this frame, it is widely accepted that less carbon-intensive alternatives might progressively replace these fuels. Thus, the obtention of liquid fuels and chemicals from gas sources through so called gas-to-liquids (GtL) and coal-to-liquids (CtL) technologies has become one of the most important and fundamental strategy [2,3]. CO and CO_2 hydrogenation to produce fuels and raw chemicals has attracted much attention in the last years [4–6]. Among these processes, Fischer–Tropsch synthesis (FTS) is a process used for reductive polymerization of CO by hydrogen for the production of organic products mainly containing hydrocarbons and at lower extent, some oxygenated products.[3].

Reported catalysts for FTS are usually active for hydrogenation reactions, that are able to form metal carbonyl during reaction conditions [7]. Typically, transition metals such as iron, cobalt, nickel and ruthenium are used for the FTS reaction, showing activity in the order Ru > Ni > Co > Fe. Despite the higher catalytic performance, ruthenium is the more expensive candidate while Ni mainly leads to methane. Therefore, Co and Fe are the industrially preferred metals for FTS processes. Though cobalt is more expensive than iron, it is reported to be more active and highly selective toward long chain hydrocarbon products.

It is widely accepted that FTS proceeds on the surface of the catalyst metal sites. However, Co is present as oxides in a freshly calcined catalyst, so catalysts should be activated through reductive treatment before reaction. Catalyst pretreatment is one of the key factors that strongly condition the activity, selectivity as well as the catalyst lifetime.

Even more, the nature of the support has important consequences for the FT performance of Co-based catalysts [8–10]. One of the key factors affecting the FTS performance is the reducibility of the catalyst which is strongly conditioned by the support since metal reducibility is closely related to metal-support interaction [11,12]. This point is particularly important for reducible support [13]. Thus, catalyst support could facilitate the crystallization and stabilization of the active metals on its texture. Moreover, physicochemical and textural properties of the support material could importantly affect the metal-support interaction, crystallite size, metal dispersion, mass transfer of the reactants/products, mechanical strength, and thermal stability of the catalyst [14,15].

Catalyst deactivation is a major challenge in both cobalt- and iron-based FTS [16,17]. The economic impact of such loss of activity justify the large industrial and academic interests in this subject. Thus, much efforts have been devoted to the comprehension of deactivation pathways, however the origin of catalyst activity decay is still under debate [18,19]. Cats *et al* pointed out that the presence of carbon deposits in re-dispersed CoNPs forming carbide entities could be possibly associated with catalytic activity lost.[17]. On the contrary, the progressive

---

formation of inactive $CoTiO_3$ upon Co spreading over TiO_2 surface has been also proposed as a possible deactivation mechanism. Indeed, if metal support interaction is too strong, TiO_{2-x} suboxide species may block active sites or $CoTiO_3$ may be formed [20]. On this basis, we could consider that the deactivating phases are $CoTiO_3$ and/or graphitic carbon deposition over metallic cobalt sites, which specifically inhibits methane formation.

In the present work we study the catalytic performance of a Co/TiO_2 system prepared by grafting over functionalized TiO_2. Comparison to classical wet-impregnated system points out interesting differences upon reduction pretreatment and subsequent reaction performance at different temperatures. These results could help to understand the importance of metal deposition on the catalyst performance for FTS reaction.

2. Experimental

2.1. Synthesis of Co/P90 catalysts

Co/TiO_2 catalysts with a nominal loading of 10 wt% Co were prepared by incipient wetness impregnation using commercial TiO_2 Evonik P90 (labelled as P90) and $Co(NO_3)_2 \cdot 6H_2O$ (Sigma Aldrich) as metal precursor. Then, the catalytic system was dried at 100 °C during 2 h and calcined in flowing air at 400 °C for 2 h. Catalyst synthesized by this method were denoted as Co/P90-WI.

For TiO_2 surface functionalization we have used 3-aminopropyltriethoxysilane (APTES). This process introduces amino- functional groups grafted at the surface of TiO_2 through ethoxy hydrolysis with surface hydroxyls forming Si-O-Ti bonds (Fig. 1). Amine functional group can act as anchor points for the metallic precursors by means of ion exchange thus obtaining a highly dispersed metal phase [21]. In a typical procedure, 1.41 mL of APTES, corresponding to a molar ratio APTES/Co (2:1), was added drop by drop to an ethanol solution containing 1 g of TiO_2. During APTES addition, the suspension was kept at 80 °C under stirring and refluxing for 24 h. Later, an ethanol solution containing cobalt precursor was added and left stirring for 1 h at 80 °C. The resulting precipitate was filtered, dried at 100 °C for 2 h and calcined in flowing air at 400 °C for 2 h. The catalysts synthesized by this method were denoted as Co/P90-F.

2.2. Characterization techniques

N_2 adsorption/desorption isotherms and BET surface area measurements were carried at 77 K using a Micromeritics Tristar II instrument. Surface areas were calculated according to the BET method. Porosity was calculated by the BJH method.

X-ray powder diffraction (XRD) patterns of the studied catalysts were obtained by using Siemens D-501 diffractometer with Ni filter and graphite monochromator and using Cu K_α radiation. The data acquisition was carried out in a 2Θ range of 10-90°, a step of 0.05°, and an acquisition time of 160 s.

Micro-Raman measurements were performed using a LabRAM Jobin Yvon spectrometer equipped with a microscope. Laser radiation (λ = 532 nm) was used as excitation source at 5 mW. All measurements were recorded under the same conditions (2 s of integration time and 30 accumulations) using a 100 × magnification objective and a 125 mm pinhole.

The reduction behaviour of the oxidised Co/TiO_2 catalysts was studied by hydrogen temperature-programmed reduction. TPR analyses were carried out using a Quantachrome Chemstar instrument equipped with a thermal conductivity detector and a mass spectrometer. About 30 mg of catalyst was first heated to 150 °C in an inert flow of Ar at 25 mL/min for 30 min before each experiment. Typically, the experiment was carried out from RT up to 900 °C using heating ramp of 10 °C/min, under fluxed 10 mL/min of 5 % H_2/Ar.

The Co content was determined by ICP-OES using an iCAP 7200 Duo spectrometer after dissolution of the solids in a microwave digester Ethos Easy.

The transmission electron microscopic (TEM) images, high angle annular dark field (HAADF) and element mapping analysis images were obtained by the equipment FEI S/TEM Talos F200S. Samples were prepared by dipping a carbon grid in the powder sample.

X-ray photoelectron spectroscopy (XPS) experiments were carried out in VG-escalab 210 equipment over pelletized samples. Samples were introduced a prechamber at 10^{-7} torr. Acquisition was performed in an appendant analysis chamber equipped with a SPECS Phoibos 100 hemispheric analyser at 10^{-9} torr using Mg Kα radiation (E = 1.5418 KeV) with 20 mA of anode current and 12 kV of potential acceleration. Ti *2p* signal (458.5 eV) was used as the internal energy reference in all the experiments.

The dispersion of the catalytic systems was calculated by means of the isotherms obtained in a volumetric chemisorption experiment with H_2. Firstly, the catalysts have been reduced at 260 °C or 400 °C and then degassed to room temperature. Once at room temperature, small amounts of hydrogen are introduced into the system, gradually increasing the pressure to 0.5 atm. The adsorbed pressure is recorded and the isotherm is obtained (total isotherm). Next, it is degassed cold again and the process is repeated, obtaining a second isotherm (weak isotherm). The calculation of the dispersion is made through the total isotherm and over the amount of total reduced cobalt in the system.

CO-DRIFT spectra were recorded with a Jasco FT-IR spectrometer equipped with liquid N_2 cooled mercury cadmium telluride (MCT) detector. In a typical experiment, few mg of the catalyst were placed in a commercial *Praying Mantis*^{TM} high-temperature environmental reaction chamber fitted with ZnSe windows for diffuse reflection spectroscopy (Harrick Scientific) and an in-situ *Praying Mantis*^{TM} diffuse reflection reaction cell (Harrick Scientific). An IR cell allowing in situ treatments in controlled atmospheres and temperatures in the range 25–400 °C. *Operando* IR experiments were performed by exposing the reduced catalysts to a flow of syngas (21 mL/min, H_2/CO 2:1) at reaction temperature and RT. The contribution from CO in the gas phase was in all cases eliminated by subtracting the corresponding spectra obtained from the
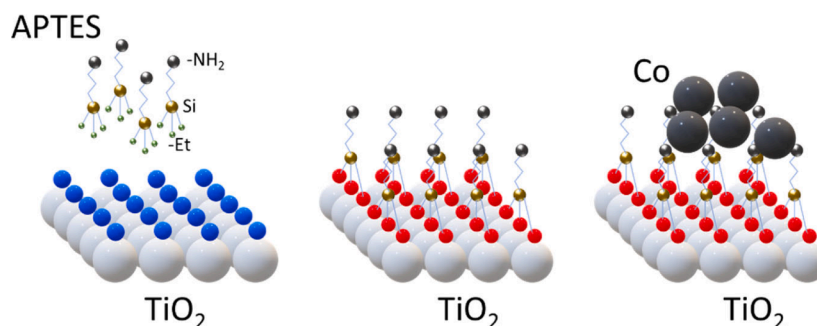

Fig. 1. Preparation flow scheme for cobalt grafting on APTES functionalized TiO_2.

bare TiO$_2$ support.

2.3. Catalytic activity in Fischer-Tropchs synthesis

The experimental measurements were accomplished with 0.25 g of catalyst diluted in 0.25 g of SiC, using a stainless-steel fixed-bed tubular reactor (300 mm length and 8 mm internal diameter) equipped with a temperature controller and four mass flow controllers. The catalysts were reduced *in-situ* by flowing H$_2$/N$_2$ (50 %) at 260 °C or 400 °C for 13 h at ambient pressure. After reduction, the temperature was lowered to 260 °C, the pressure was increased up to 1.0 MPa and CO was introduced. Syngas with H$_2$/CO molar ratio of 2 (CO:H$_2$:N$_2$ volume ratio of 1:2:2, N$_2$ as internal standard for gas chromatography) was flowed at 35 mL/min through the reactor at constant gas hourly space velocity (GHSV) of 4180 h^{-1} considering the catalyst bed volume. The reaction is monitored during 6 h, reaching the pseudo-steady state. Heavier hydrocarbons traces were condensed in a trap located at the reactor outlet and kept at 100 °C. Reaction products were analyzed by means of a previously calibrated GC (Agilent 7820) equipped with two columns and TCD and FID detectors. All lines connecting the reactor and GC were heated in order to avoid condensation of products.

Conversion and selectivity values were calculated using the following equations:

$$Conversion(\%) = \frac{[CO]_t}{[CO]_i} \times 100 \qquad (1)$$

where $[CO]_t$ represents the moles of reacted carbon monoxide and $[CO]_i$ the initial carbon monoxide amount.

$$Selectivity\ to\ product\ i(\%) = \frac{[product_i]_t \times n_i}{\sum [product_i]_t \times n_i} \times 100 \qquad (2)$$

where $[product_i]_t$ represents the moles of the specific product; n_i the number of C atoms in the product molecule, and $\sum [product]_i$ the sum of moles from all products in the reaction. Product selectivities are expressed on a carbon basis.

3. Results and discussion

3.1. Characterization of the Co/TiO$_2$ catalysts

3.1.1. Structural and textural properties

The XRD patterns of the support and calcined Co/TiO$_2$ catalysts are shown in Fig. 2. TiO$_2$-P90 support shows peaks corresponding to anatase phase. The structure of support did not experience significant variation upon addition with metal precursor and calcination. No changes in the

support are either observed after synthesis with APTES. Besides TiO$_2$ peaks, reflections belonging to the Co$_3$O$_4$ spinel phase are clearly perceived in the impregnated Co/P90-WI catalyst, with no signs for the presence of other crystalline cobalt phases [22,23]. However, the low intensity of the observed spinel peaks which overlap with TiO$_2$ diffractions avoid the correct calculation of the Co$_3$O$_4$ crystallite sizes from line broadening. In the case of functionalized Co/P90-F catalyst, peaks corresponding to the cobalt spinel phase is not observed, denoting a less content of this phase, lower crystalline size or amorphous situation.

Raman spectra in the range of 50–1000 cm^{-1} for Co/P90 catalysts are reported in Fig. 2.b. Accordingly to XRD patterns, Raman bands at 144, 200, 400, 520 and 640 cm^{-1}, corresponding to anatase's E$_g$(ν_6), E$_g$(ν_5), B$_{1g}$(ν_4), A$_{1g}$(ν_3)−B$_{1g}$(ν_2), and E$_g$(ν_1) modes were observed in all catalysts. The anatase E$_g$(ν_6) Raman peak at ca 144 cm^{-1} is the most intense and largely the most investigated in the literature [24–27]. Several works focus on the variation of position, width, and shape of this peak in relation to several structural effects such as defects in the stoichiometry, phonon confinement, extrinsic doping, presence of minority phases, etc. In our case, the shifting of this E$_g$ peak of anatase could be associated to the formation of new bonds due to the presence of Co and/ or Si, by disturbing the Ti–O–Ti bonds in the crystal lattice. The observed blue shift in the E$_g$ peak could be due to increasing structural strain in unit cell. Thus, E$_g$ Raman peak for Co/P90-F is clearly shifted, showing less intensity. Indeed, the peak shift and the diminution of peak intensities has been related to the presence of crystal strain and non-stoichiometric defects [28].

The acquired spectra for Co/P90-WI and Co/P90-F catalysts also show the appearance of new peaks at 472 cm^{-1}, 612 cm^{-1} and 680 cm^{-1} that can be attributed to E$_g$, F$_{2g}$ and A$_{1g}$ modes assigned to Co$_3$O$_4$, as reported in the literature [29]. It can be noticed that in the case of Co/ P90-WI catalyst such peaks appear with stronger intensity, denoting a clearer formation of the spinel structure in this catalyst. Though spinel phase was not detected from XRD, we evidenced the presence of spinel peaks in the Raman spectrum for Co/P90-F. We must highlight that Raman spectroscopy is very sensitive and we could notice the occurrence of crystalline structures even at low content [30]. Although Raman spectral fingerprints of Co$_3$O$_4$ have been well established, both Raman and infrared spectra of CoO is less understood. Thus, the room-temperature Raman spectrum of CoO is essentially dominated by a broad band at ca. 1000 cm^{-1}, which is consistent with the expected second-order Raman scattering from optical modes in CoO [31]. This broad band for CoO is not clearly detected in our case. Indeed, at room temperature, no Raman-active phonon line is observed, which is in agreement with the selection rule for rock-salt CoO [31].

As observed from XRD and Raman spectroscopy a greater amount of cobalt spinel species in the WI catalyst with respect to F one could be
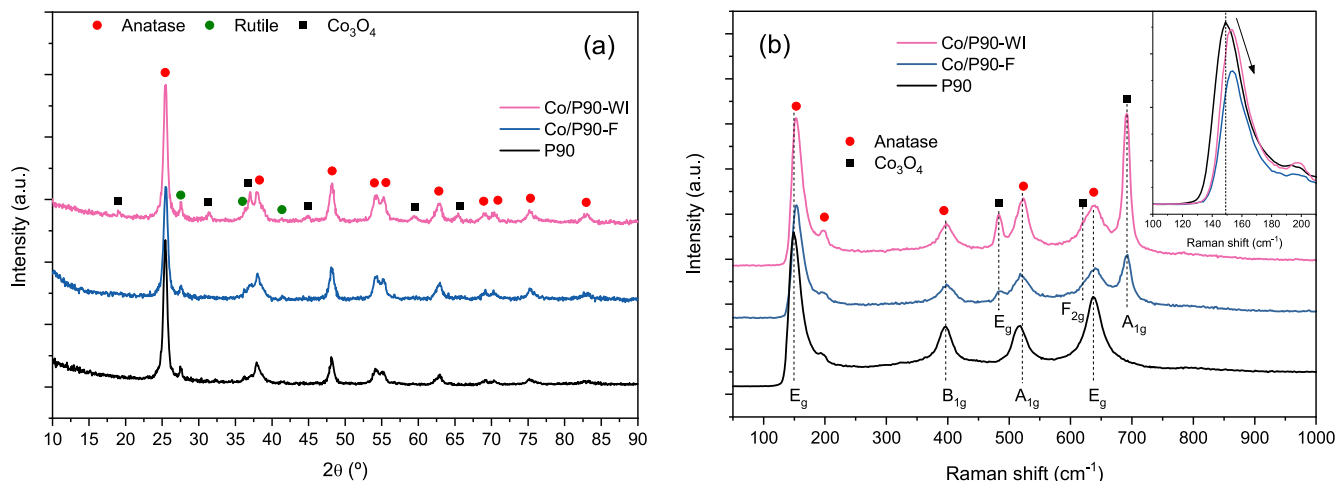

Fig. 2. a) X-ray diffraction patterns and b) Raman spectra of TiO$_2$-P90 and Co/P90 catalysts.

inferred. However, by observing the chemical composition from ICP analysis (Table 1), the amount of Co in both systems is similar, pointing out the efficiency of grafting procedure over functionalized P90 support. From the observed results, we clearly infer that the unlike spinel phase content in both catalysts is not related to a different Co content.

Derived textural properties from N_2 adsorption isotherms are summarized in Table 1. TiO$_2$ P90 support shows a type III adsorption isotherm typical for mesoporous solids (not shown). At high relative pressures (>0.90) a rapid increase in the amount of N_2 adsorbed is observed, denoting the presence of large interparticle mesopores and macropores. TiO$_2$ P90 support exhibits a notably higher specific surface area (101 m^2/g). Both Co/P90 catalysts show similar N_2 adsorption isotherms, however BET surface area shows important changes depending on the deposition method. Thus, for WI catalyst an important decrease in BET is observed with respect to the value of the support. Such diminution can be due to the deposited metal oxide phases on TiO$_2$ surface. On the contrary, functionalized catalyst shows only a slight decrease in BET surface area with respect to bare support. This surface area diminution was already observed in the literature and was explained by considering that APTES also penetrated inside the pores, rather than only dispersing on the external surface [32]. However, further deposition of cobalt does not affect to the surface area as in the case of impregnated catalyst.

By observing the pore size distribution (Fig. 3) different cobalt deposition induces clear modifications in the pore features. Thus, by wet impregnation it is evidenced that the initial pore distribution of pristine P90 is lost, arising a new pore size family at ca 10 nm. This new pore feature can be associated to the covering of cobalt cluster on P90 surface. On the other hand, functionalized catalyst also shows the disappearance of the lower size pore family observed for P90. However, it is observed the evolution of certain mesoporosity with a new family of pores at 20 nm diameter size. This fact could be related to the formation of hierarchical silicon mesoporous structure over P90 which could develop the observed mesoporosity.[32].

3.1.2. Reducibility and particle size of cobalt

In order to study the reducibility of the Co-based catalytic systems, a study was carried out by H$_2$-TPR and the corresponding reduction profiles are presented in Fig. 4. Thus, Co/P90-WI catalyst presents a bimodal profile denoting two different reduction processes at ca 400 °C and 520 °C, which can be respectively associated to the well-known two-step reduction of Co$_3$O$_4$ to Co^0 (Co$_3$O$_4$ → CoO; CoO → Co^0)[33].

In the functionalized Co/P90-F system, two clear changes are observed in the reduction profile with respect to Co/P90-WI system. Firstly, the two peak profile observed for WI catalyst is also observed in the F catalyst, however showing much less intensity. Noteworthy is the appearance of a new reduction process in Co/P90-F at higher temperature, ca 615 °C. This new peak could be associated with a new cobalt phase that would be anchored on the surface created by APTES on the support, with a strong interaction between cobalt and silicon from the functionalizing agent [34].

The calculated H$_2$ consumption from TPR profiles gives important differences, so different cobalt crystalline situation can be inferred [35]. Considering the calculated H$_2$ consumption (1.9 mmol/g$_{cat}$ and 1.5 mmol/g$_{cat}$ for Co/P90-WI and Co/P90-F respectively) we could deduce that cobalt is mainly present as Co$_2$O$_3$ for Co/P90-WI while CoO would be the major phase for Co/P90-F. Therefore, deposition over
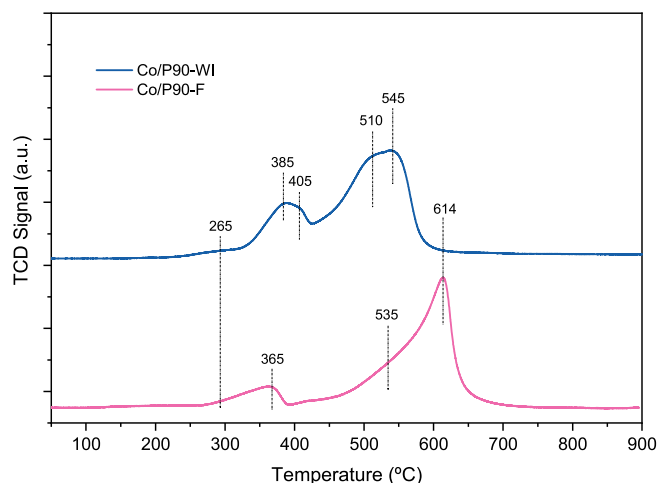
Table 1
Chemical composition and textural properties of Co/P90 catalysts.

Catalyst	Co wt% *	S$_{BET}$ (m^2/g)	Pore volume (cm^3/g)	Pore size (nm)
P90	—	101	0.23	3 + 30
Co/P90-WI	9.5	75	0.23	10
Co/P90-F	8.9	95	0.35	2 + 30

* From ICP analysis.
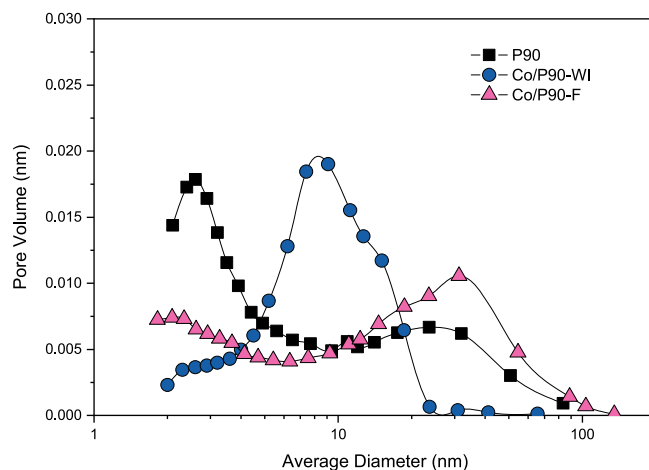
Fig. 3. Pore size distribution of P90 support and calcined Co/P90 catalysts.

Fig. 4. H$_2$-TPR profiles for the Co/P90 catalysts.

functionalized TiO$_2$ strongly conditions the structural features of supported cobalt.

In order to study the effect of different reduction treatment temperatures on Co/P90 catalyst, we have also performed the TPR analysis over reduced catalyst (Figure S1). As we have discussed before, Co/P90-WI and Co/P90-F catalysts also showed different evolution upon reduction. Low temperature reduction over Co/P90-WI leads a completely different TPR with respect to Co/P90-F catalyst. Thus, only one TPR peak at ca 420 °C is observed for reduced Co/P90-WI catalyst. This implies not only the expected disappearance of the Co species reducing at ca 350 °C but also the lowering of the reduction temperatures of Co species reducing at ca. 550 °C from the pristine TPR profile (Figure S1). Such shift to lower reduction temperature would point out a clear SMSI effect as well as certain modification of the metal dispersion features that induces the reducibility behaviour. From the H$_2$ consumption, 45 % of total Co is reduced at 260 °C. After reduction at 400 °C, almost the whole Co got reduced.

As pointed out from Fig. 4, Co/P90-F shows a different reduction behavioural feature. The first important issue is that reduction at 260 °C leads to a lower reduction degree of Co species (only 18 % vs 45 % showed by Co/P90-WI), being the TPR profile similar as the pristine one. It is worthy to note that in this case, the observed modification of reducibility of the unreduced Co species is not observed, denoting the important effect of surface functionalization. Furthermore, the after reduction at 400 °C, it is possible to find a fraction of Co unreduced,

denoting that in this case Co are hardly reduced. Reduction degree calculated in this case is 74 % (vs 98 % showed by Co/P90-WI reduced at 400 °C).

The HAADF-STEM images of the calcined Co/P90 catalysts are shown in Fig. 5. In the WI system it can be observed how cobalt particles appear with a varied particle size range, between 15 and 30 nm. However, in the F catalyst, a large dispersion of the cobalt phase was observed throughout the TiO$_2$ surface. This highly dispersed Co species would be anchored on the surface to the silicon network formed during the functionalization of the support. In this sense, it has been reported that high Co loading would cause cobalt particles aggregation and the lowering of the number of active sites, which results in a low FTS activity [36]. Therefore, preparation of catalyst with not only high Co loading but also superior metal dispersion is crucial to achieve high FTS activity.

3.1.3. Surface properties and cobalt dispersion

The surface properties of cobalt in the catalytic systems have been studied by XPS and FTIR. In Fig. 6 we have depicted the Co2p signal from XPS analysis for both Co supported catalysts. As can be seen, Co2p curve for Co/P90-WI can be decomposed in two contributions centered at binding energies of 779.3 eV and 781.5 eV that could be ascribed respectively to Co^{3+} (corresponding to spinel Co$_3$O$_4$) and Co^{2+} (associated to CoO as well as Co$_3$O$_4$) [37–40]. However for, Co/P90-F only Co^{2+} can be envisaged.

Besides, as reported in the literature, Co$_3$O$_4$ exhibits a weak shake-up satellite at higher binding energies (around 10 eV from the main peak) while CoO has a characteristic strong satellite at 786 eV (around 6 eV above the main peak)[41]. From the relative areas of deconvoluted peaks (Table 2), we have estimated 68 % of spinel content for Co/P90-WI while only CoO would be present in CoP/90-F.

This result firmly agrees with the previous H$_2$ consumption from TPR, and with the observation from XRD and Raman results (Fig. 2). Furthermore, the different structural features observed between the Co-based catalysts could be also correlated with the diminution in the bimodal reduction profile in Co/P90-F catalyst obtained from TPR.

Another important information that can be outlined concerns the important difference in the intensity of Co2p signal for Co/P90-WI and Co/P90-F. Thus, considering the surface Co/Ti ratio calculated (Table 2), a large increase is observed between Co-supported catalysts, going from 0.08 to 0.39 for Co/P90-WI and Co/P90-F respectively. Considering the similar Co content obtained from ICP, this data would confirm the highest dispersion on surface for the functionalized systems
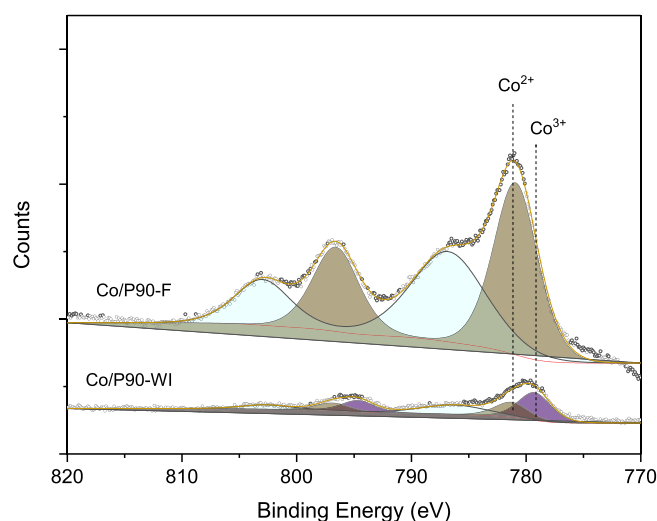

Fig. 6. Co2p signal from XPS analysis for Co/P90 catalysts.

Table 2
Surface chemical analysis from XPS for Co/P90 catalyst.

Catalyst	Co at%	Co^{3+}at%	Si at%	Co/Ti	Co/Si	Si/Ti
Co/P90-WI	1.7	46	—	0.08	—	—
Co/P90-F	7.5	0	4.5	0.39	1.67	0.22

that we highlighted by transmission microscopy (Fig. 5).

In order to verify the influence of the reduction pretreatment temperature on the dispersion of the metallic phase on the catalysts, a study of H$_2$ chemisorption was carried out in Co-supported systems, after reducing at operating temperatures (260 °C and 400 °C) for 13 h (Figure S2). We firstly need to know the amount of metallic cobalt present in the samples after each reduction process. Thus, metallic Co was obtained by difference from TPR measured after the reduction process for 13 h up to 900 °C. The results of both experiences are reflected in Table 3.

Looking at the degrees of cobalt reduction values obtained, it is observed that, after treatment at low temperature (260 °C), a low percentage of reduced cobalt is present in Co/P90-F (18 %) compared to
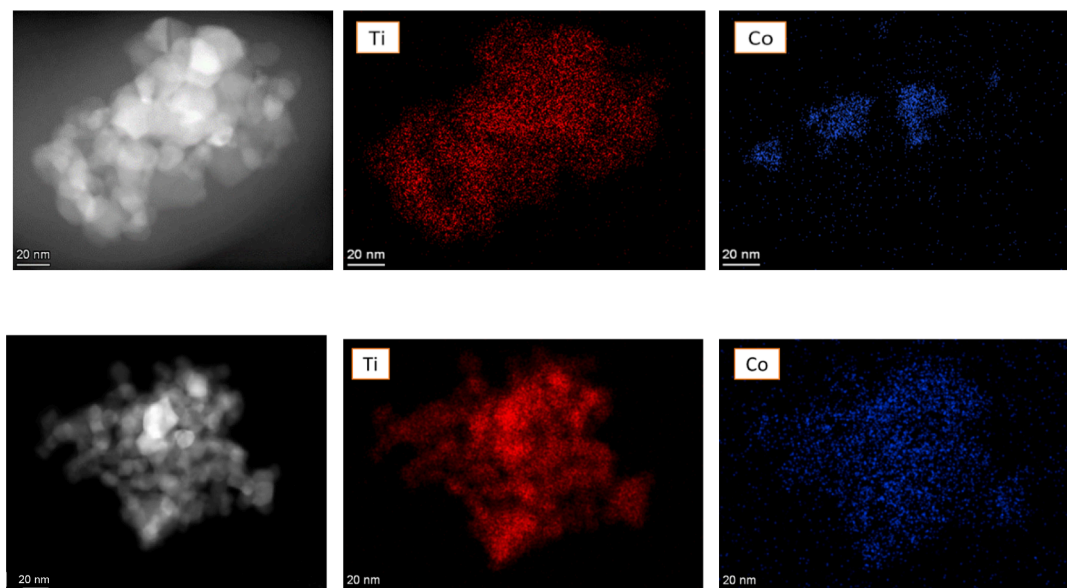

Fig. 5. A representative HAADF-STEM images of the a) Co/P90-WI (*upper panel*) and b) Co/P90-F (*lower panel*) catalysts.

Table 3
Metal dispersion of cobalt in the Co/P90 catalysts.

Catalyst	Reduction degree to Co^0 (%)[a]		Metal dispersion (%)[b]	
	Red 260 °C	Red 400 °C	Red 260 °C	Red 400 °C
Co/P90-WI	45	98	1.3	0.2
Co/P90-F	18	74	1.1	1.1

[a] Percentage degree of cobalt reduction upon treatment in H_2 at different temperatures for 13 h.

[b] Metallic dispersion of cobalt calculated by hydrogen chemisorption uptake over Co^0 sites.

that for Co/P90-WI (45 %). This difference can be understood considering the reduction profile of the catalytic systems (Fig. 4). As discussed above, one of the effects of the synthesis with APTES was the diminution of bimodal reduction process at temperature below 600 °C. Thus, in functionalized systems after reduction at 260 °C for 13 h, only this first reduction process has been completed. On the other hand, in the impregnated systems both reduction processes overlap, therefore, the kinetic effect after 13 h of reduction means that part of the cobalt involved in the reduction process at higher temperature has also been reduced. Based on the data obtained after the reduction process at high temperature (400 °C) for 13 h, it is observed that practically all the metallic phase is reduced in the impregnated catalysts, however, only around 74 % of the cobalt has been reduced in functionalized catalysts. This difference is explained considering that not all the cobalt that reduces at high temperature (around 615 °C) in the functionalized systems has been reduced upon treatment at 400 °C after 13 h. Based on these results, it can be argued that the impregnated catalyst presents a better

reducibility than the catalysts functionalized with APTES.

The metallic dispersion (MD) obtained by H_2 pulse chemisorption shows a higher percentage of Co^0 dispersion for the WI catalyst after reduction at low temperature (Table 3). However, it is interesting to observe that the dispersion values of the metallic phase in these system decreases severely when the reduction treatment is carried out at high temperature, obtaining values 0.2 % for Co/P90-WI. This loss of around 85–90 % of dispersion would be correlated to loss of metallic sites which take place during the reduction stage a high temperature. In this process, due to the strong metal interaction (SMSI), partially reduced TiOx species would migrate on top of the Co^0 particles, partially covering them and thus suppressing their H_2 (and CO) chemisorption capacity. On the other hand, it is interesting to observe how in the functionalized catalyst the dispersion remains constant independent of the reduction temperature, obtaining a value of 1.1 % irrespective of the reduction temperature. The fact that the temperature is not significant in the dispersion of the metallic phase confirms the presence of the Co^{2+} species bound to the surface silicon from APTES grafting, which is partially reduced to Co^0 at 400 °C, avoiding the coverage of the TiOx species and therefore exposed as active centers for the Fischer-Tropchs reaction.

The implication of the differences in the physicochemical characteristics of these systems, described so far, in the catalytic performance for the Fischer-Tropchs reaction are discussed in the next section.

3.2. Catalytic studies for Fischer-Tropsch synthesis reaction.

The catalytic activity of the studied systems is shown in Fig. 7. Co/P90 catalytic systems were tested in FTS reaction after each of the two reduction processes. After reduction at low temperature (260 °C) two
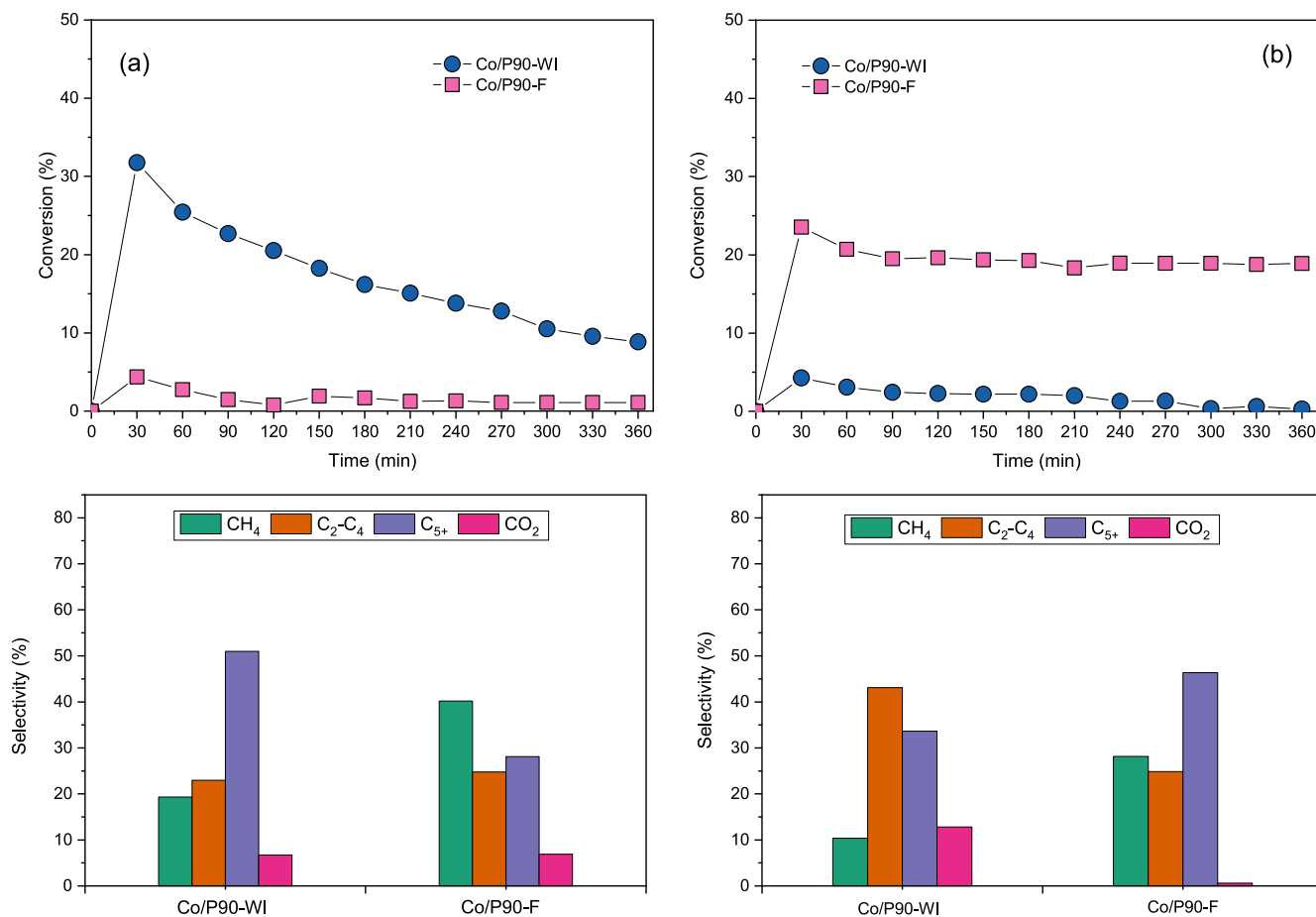
Fig. 7. CO conversion rate and product selectivities in Fischer-Tropchs reaction after reduction at a) 260 °C and b) 400 °C. Constant reaction conditions: 0.25 g of catalyst diluted in 0.25 g of SiC. At 260 °C and 1 MPa, CO: H_2: N_2 = 1:2:2, GHSV = 1800 h^{-1}.

different behaviours are noticed. The impregnated catalyst presents a conversion maximum at short reaction times, followed by a significant and progressive deactivation along TOS. Since at this temperature SMSI would not be expected, such important deactivation could be caused by the progressive deposition of coke or even the formation of inactive oxidic species.

On the other hand, the functionalized system shows a great stability during the 6 h from short reaction times. In general, after 6 h of TOS, the functionalized catalyst presents a lower catalytic activity than the impregnated system, showing conversions of 2 % and 9 % respectively. As explained above, in the functionalized system, when reducing at low temperature, only an 18 % degree of cobalt reduction is obtained, and at this temperature, the identified species of Co^{2+} that are bound to the surface silicon have not yet begun to reduce. Therefore, they would not be available to participate in the reaction. Therefore, only cobalt that has not been anchored by the functionalizing agent and located on the TiO_2 surface would participate under these conditions. In this way, the difference in activity between the functionalized and impregnated catalysts could be explained by the amount of active phase (Co^0) available after the reduction process, this being greater for the WI systems with respect to the F systems (Table 2), as discussed above.

After reduction at high temperature (400 °C), Co/P90-WI shows significantly lower CO conversion and a practical complete deactivation at the end of the catalytic run, passing the conversion from 4 % to 1 %. Despite having almost 100 % of cobalt as Co^0 under these conditions (Table 2), the enormous decrease in the conversion of CO would reveal the negative effect of SMSI for the activity of the system, inhibiting the adsorption of the reagents in the metal centers, as mentioned previously [42]. On the contrary, in spite of the lower amount of metallic Co^0, Co/P90-F catalyst notably improves their catalytic performance after reduced at higher temperature, going from 2 % to ca 20 % for reduction at 260 °C and 400 °C respectively. Thus, we could conclude that APTES functionalization of the TiO_2 support leads to the formation of a cobalt species in the surface layer of the functionalizing agent, which would remain unaffected by the SMSI effect after reduction at high temperature. Moreover, the observed stability clearly points out that deactivation shown for Co/P90-WI at lower reduction temperature is not taking place in this case either. Regarding to the obtained product fractions, it can be pointed out that similar selectivities to C_{5+} is attained for Co/P90-WI reduced at 260 °C and Co/P90-F reduced 400 °C. It is noteworthy that, unlike in the case of Co/P90-WI reduced at 260 °C, Co/P90-F reduced at 400 °C shows a stable conversion rate with similar C_{5+} selectivity. We have also to mention that methane selectivity is also notable. This could be due to the lower cobalt cluster size which would favour methane formation [43]. By observing the evolution of product selectivities with TOS for Co/P90-WI reduced at 260 °C and Co/P90-F reduced at 400 °C (Figure S2), we can observe that for Co/P90-WI catalyst selectivity to C_{5+} initially grows till reaching a stable value. At this point of stable selectivity, conversion drops drastically (Fig. 7). At the same time CH_4 and CO_2 selectivities decay. This initial step coincides with highest conversion values. On the contrary, Co/P90-F catalyst reduced at 400 °C shows a stable conversion rate along TOS. Moreover, C5+ selectivity appears also stable during the whole reaction time (Figure S2).

Regarding to CO_2, it seems that S_{CO2} clearly diminished for Co/P90-F catalyst at 400 °C (Fig. 7). In this sense, it has been widely accepted that CO_2 formation during FT synthesis is related to both, from the WGS reaction as well as from the Boudouard reaction [44,45].

Furthermore, it can be argued that low CO conversion might result in an extremely small amount of the formed H_2O on catalyst surface, which subsequently may hinder WGS reaction. As above mentioned, besides WGS reaction, the Boudouard reaction is the second possible way to produce CO_2. On this basis, we cannot discard the CO_2 formation via CO disproportionation reaction. In this sense, the particular Co dispersion on Co/P90-F after reduction at 400 °C could disfavour WGS. Indeed, it has been reported that the WGS activity would increase as the cobalt

cluster size increases [46].

In Fig. 8 we show the evolution of DRIFT spectra under operando conditions for Co-based catalysts after reduction at 400 °C. A complex group of IR bands corresponding to various species appear and evolve under different conditions studied. The presence of methyl and methylene groups belonging to various hydrocarbons is confirmed by the bands in the range between 1510 and 1300 cm^{-1}, corresponding to the C—H asymmetric and symmetric bends (δ-as and δ-s)[47,48]. Moreover, methane typical rotovibrational bands centered at 1305 cm^{-1} is also present in both cases, being prominent for Co/P90-F catalyst [49].

Band at 1589 cm^{-1} and two other bands at 1373 cm^{-1} and 1360 cm^{-1} are assigned to asymmetric $\nu_{as}(COO–)$ and symmetric $\nu_s(COO–)$ vibrations of carbonate and formate species on the catalyst surface [50–53]. The presence of surface carbonate/bicarbonate species suggests that CO_2 was produced during CO adsorption. Noteworthy, these surface carbonates seems to be produced at less extent for Co/P90-F catalyst.

All these bands clearly denote the formation of different hydrocarbons during reaction that remains adsorbed when CO/H_2 mixture stopped and catalyst is purged with He.

When the syngas stream is set at room temperature, a complex group of bands arise in the range 2100–1900 cm^{-1} only in the case of Co/P90-F. Bands within this region would correspond to CO adsorbed on heterogeneous metallic sites forming different carbonyl species [54,55]. From the previous literature, the stretching frequencies of cobalt carbonyl complexes were recorded below 2050 cm^{-1} for metallic cobalt, 2070–2110 cm^{-1} for Co^+, 2120–2170 cm^{-1} for Co^{+2}, and 2178–2180 cm^{-1} for Co^{+3} [56]. Thus, carbonyl bands observed for Co/P90-F would be ascribed to Co^0 and Co^+ species.

We must highlight the lack of such kind of bands on Co/P90-WI that clearly points out the absence of exposed metallic sites. This result reinforces the previous stated loss of Co active sites due to SMSI effect after reduction at 400 °C, and the subsequent progressive decay in the CO conversion.

The study of the spent catalyst by TEM also confirms the different evolution of Co/P90 catalyst during reaction (Figs. 9 and 10). As we have argued, functionalization leads to a better catalyst stability by hindering the SMSI after reduction at high temperature with the subsequent loss of Co active sites. The absence of Co-carbonyl bands on Co/P90-WI reduced at 400 °C clearly demonstrates the coverage of metallic sites. The evolution of active sites during reaction has been evidenced by observing the images of the spent catalyst (Fig. 9). In the impregnated catalyst we have shown the formation of Co agglomerates easily distinguishable in Fig. 5. After reaction, these agglomerates seem to be disappeared and good dispersion of cobalt cluster is attained. This fact was already anticipated from the TPR after reduction for this catalyst. Indeed, the lack of cobalt carbonyls points out the absence of exposed metallic sites. Such Co redispersion after FT reaction has been previously described by some authors [12,57].' Cats *et al* argued that cobalt agglomerates would be dispersed on the surface through surface oxidation or surface carbide formation. Such process would be opposite to expected "classical" SMSI effect. On the other side Qiu *et al* proposed a dispersion mechanism forming fried-egg-like cobalt entities which would lead to higher activity [12]. Similar behavior has been described by our group in a Ni/CeO_2 system, where the metallic particles seem to be flattened and buried in this case as a consequence of the SMSI effect [58]. Thus, a clear metallic species migration/dispersion was induced by SMSI in Co/P90-WI after soft reduction at 260 °C through the formation of hydride-like entities of the partially reduced support, which account for a high mobility of the phases [59]. However, if the spreading becomes extensive, it manifests in more nonreducible $CoTiO_3$ formed, which is likely to lead to a decrease in catalytic activity. In both cases, the observed migration and spreading of Co nanoparticles forming either oxidic or carbidic species would be implicated in deactivation of Co FTS catalysts.

The situation for Co/P90-F after reaction is certainly surprising
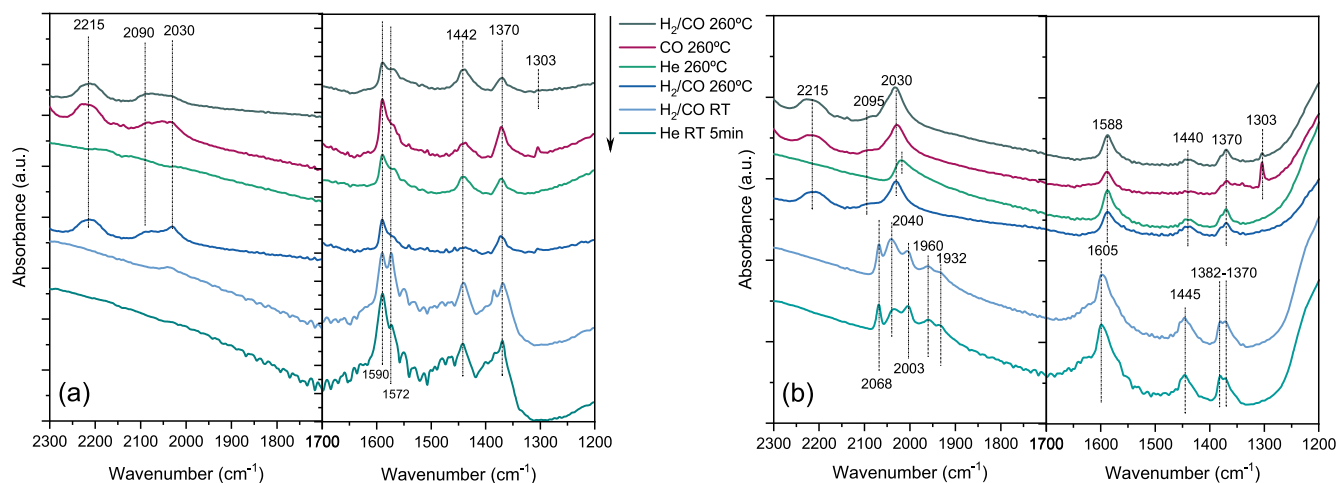
Fig. 8. Evolutions of the *operando* DRIFT spectra (background subtracted) at different reaction conditions for a) Co/P90-WI and b) Co/P90-F catalysts H_2-reduced at 400 °C for 13 h.
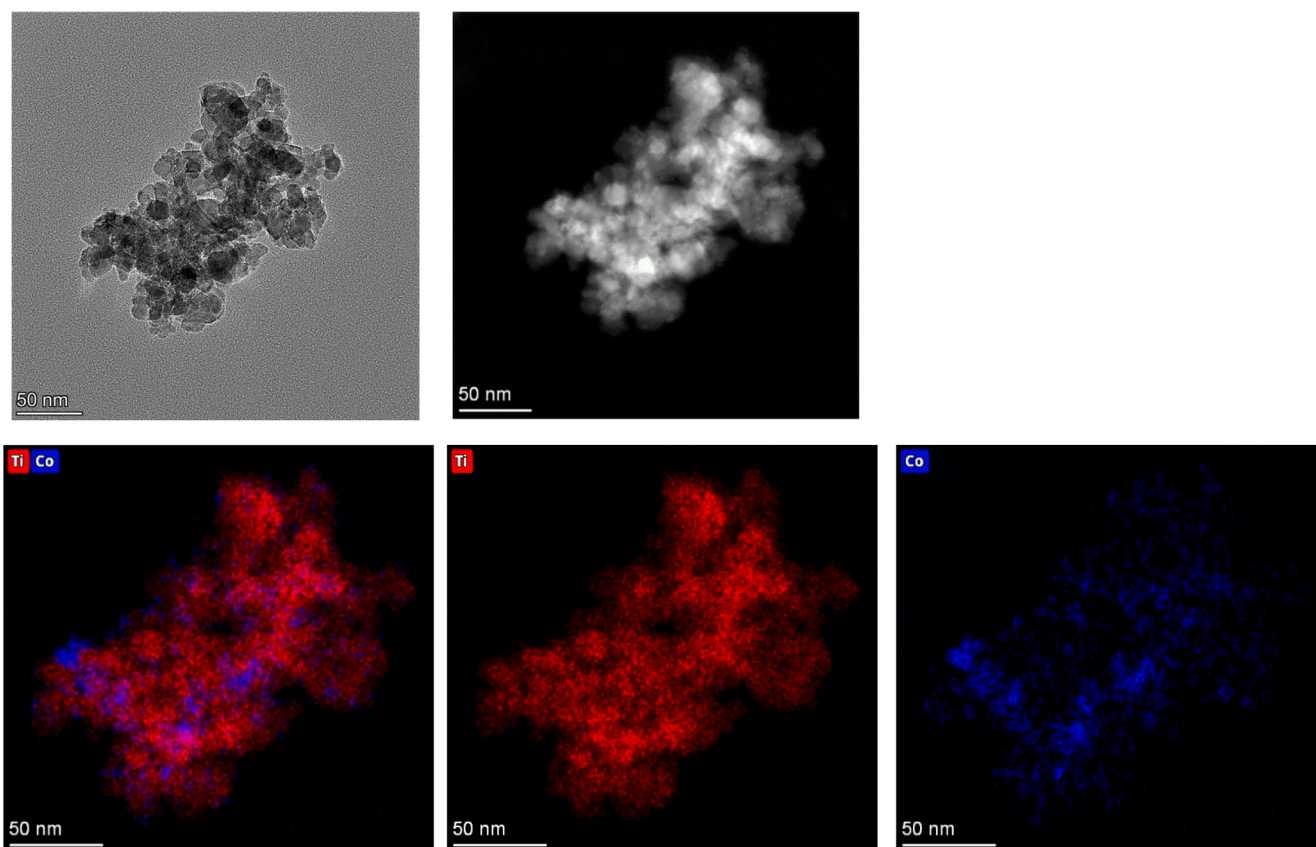
Fig. 9. STEM HAADF images for Co/P90-WI reduced at 400 °C post-reaction at 260 °C.

(Fig. 10). As we have shown for Co/P90-F fresh catalyst, Co appeared well dispersed over TiO_2 (Fig. 5). However, after reaction cobalt entities seem to be more agglomerated forming bigger clusters in close interaction with silicon (Fig. 10). Despite the observed agglomeration, the occurrence of Co-carbonyls denotes that they remain exposed maintaining the catalytic activity. Therefore, upon reduction at 400 °C SMSI effect is hampered leading to more reduced Co with high stability against deactivation under reaction.

4. Conclusions

We have prepared two Co/TiO_2 catalysts by wet impregnation (Co/P90-WI) and grafting over functionalized TiO_2 (Co/P90-F). Immobilization of cobalt over APTES grafted TiO_2 induces important surface and structural modifications. Furthermore, significant differences on the catalytic performance has been subsequently observed for Fischer-Tropsch synthesis reaction. Co/P90-WI catalyst shows a better conversion rate after reduction at 260 °C, however important deactivation is observed achieving a final CO conversion rate of 10 %. For Co/P90-F catalyst reduced at 260 °C the presence of silicon hinders the
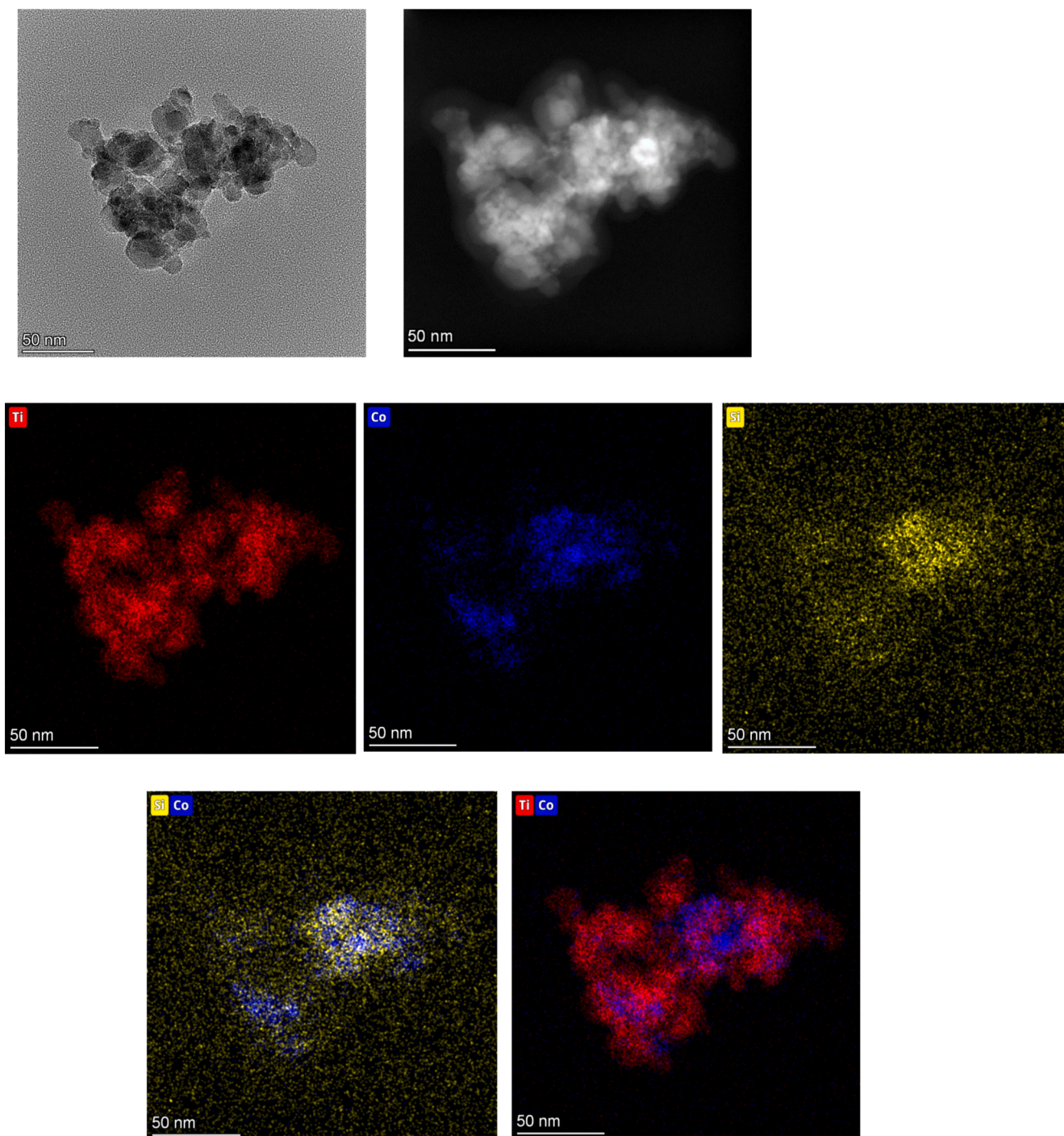
Fig. 10. STEM HAADF images for Co/P90-F reduced at 400 °C post-reaction at 260 °C.

reduction of cobalt and leading to a low number of active sites for the reaction and a much lower conversion.

Though reduction at higher temperature leads to a higher number of metallic sites in the Co/P90-WI, the catalytic activity decreased importantly reaching an almost negligible final conversion. On the contrary, Co/P90-F system showed better CO conversion rates after reduction at 400 °C, being in addition highly stable during the reaction time with high selectivity to C_{5+}. From the study of the fresh and spent catalysts, we have demonstrated that reduction at high temperature strongly affects to Co/P90-WI catalyst. Though almost complete reduction and certain redispersion of cobalt is achieved, important SMSI leads to active sites coverage and the loss of catalytic activity. Co/P90-F catalyst

showed notable improvement after reduction at 400 °C with a conversion of 20 %. Initial highly disperse Co sites evolves to certain agglomeration upon reduction at 400 °C. But in this case, Co metallic sites are in close interaction to silicon which protect against SMSI and even from catalyst deactivation by hindering the formation of inactive oxidic species.

CRediT authorship contribution statement

Francisco Platero: Methodology, Investigation, Writing – original draft. **Alfonso Caballero:** Conceptualization, Methodology, Supervision. **Gerardo Colón:** Conceptualization, Methodology, Writing –

original draft, Writing – review & editing, Supervision.

Declaration of Competing Interest

The authors declare that they have no known competing financial interests or personal relationships that could have appeared to influence the work reported in this paper.

Data availability

Data will be made available on request.

Appendix A. Supplementary data

Supplementary data to this article can be found online at https://doi.org/10.1016/j.fuel.2023.127528.

References

[1] Ang TZ, Salem M, Kamarol M, Das HS, Nazari MA, Prabaharan N. A comprehensive study of renewable energy sources: Classifications, challenges and suggestions. Energy Strategy Rev 2022;43:100939.

[2] Grim RG, To AT, Farberow CA, Hensley JE, Ruddy DA, Schaidle JA. Growing the Bioeconomy through Catalysis: A Review of Recent Advancements in the Production of Fuels and Chemicals from Syngas-Derived Oxygenates. ACS Catal 2019;9:4145–41723.

[3] Martinelli M, Gnanamani MK, LeViness S, Jacobs G, Shafer WD. An overview of Fischer-Tropsch Synthesis: XtL processes, catalysts and reactors. Appl Catal A: Gen 2020;608:117740.

[4] Chen G, Waterhouse GIN, Shi R, Zhao J, Li Z, Wu LZ, et al. From Solar Energy to Fuels: Recent Advances in Light-Driven C1 7Chemistry. Angew Chem Int Ed 2019; 58:17528–755.

[5] Du C, Lu P, Lu P, Tsubaki N. Efficient and New Production Methods of Chemicals and Liquid Fuels by Carbon Monoxide Hydrogenation. ACS Omega 2020;5:49–56.

[6] Xu D, Wang Y, Ding M, Hong X, Liu G, Tsang SCE. Advances in higher alcohol synthesis from CO2 hydrogenation. Chem 2021;7:849–81.

[7] Teimouri Z, Abatzoglou N, Dalai AK. Kinetics and Selectivity Study of Fischer-Tropsch Synthesis to C5+ Hydrocarbons: A Review. Catalysts 2021;11:330.

[8] Ishihara T, Horiuchi N, Eguchi K, Arai H. The Effect of Supports on the Activity and Selectivity of CoNi Alloy Catalysts for CO Hydrogenation. J Catal 1991;130: 202–11.

[9] Munirathinam R, Minh DP, Nzihou A. Effect of the Support and Its Surface Modifications in Cobalt-Based Fischer−Tropsch Synthesis. Ind Eng Chem Res 2018; 57:16137–61.

[10] Valero-Romero MJ, Rodríguez-Cano MA, Palomo J, Rodríguez-Mirasol J, Cordero T. Carbon-Based Materials as Catalyst Supports for Fischer-Tropsch Synthesis: A Review. Front Mater 2021;74:617432.

[11] Borg Ø, Eri S, Blekkan EA, Storsæter S, Wigum H, Rytter E, et al. Fischer-Tropsch Synthesis over γ-Alumina-Supported Cobalt Catalysts: Effect of Support Variables. J Catal 2007;248:89–100.

[12] Qiu C, Odarchenko Y, Meng Q, Cong P, Schoen MAW, Kleibert A, et al. Direct observation of the evolving metal–support interaction of individual cobalt nanoparticles at the titania and silica interface. Chem Sci 2020;11:13060–70.

[13] Hernandez Mejía C, van der Hoeven JES, de Jongh PE, de Jong KP. Cobalt−Nickel Nanoparticles Supported on Reducible Oxides as Fischer−Tropsch Catalysts. ACS Catal 2020;10:7343–54.

[14] Qi Z, Chen L, Zhang S, Su Ji, Somorjai GA. A mini review of cobalt-based nanocatalyst in Fischer-Tropsch synthesis. Appl Catal A: Gen 2020;602:117701.

[15] ten Have IC, Weckhuysen BM. The active phase in cobalt-based Fischer-Tropsch synthesis. Chem Catalysis 2021;1:339–63.

[16] Tsakoumis NE, Rønning M, Borg Ø, Rytter E, Holmen A. Deactivation of cobalt based Fischer-Tropsch catalysts: a review. Catal Today 2010;154:162–82.

[17] Cats KH, Weckhuysen BM. Combined operando X-ray diffraction/Raman spectroscopy of catalytic solids in the laboratory: the Co/TiO2 Fischer-Tropsch synthesis catalyst showcase. ChemCatChem 2016;8:1531–42.

[18] . A. Carvalho, V.V. Ordomsky, Y. Luo, M. Marinovac, A.R. Muniz, N. Romeu Marcilio, A.Y. Khodakov. Elucidation of deactivation phenomena in cobalt catalyst for Fischer-Tropsch synthesis using SSITKA, J. Catal. 344, (2016), pp. 669-679.

[19] Bartholomew CH, Rahmati M, Reynolds MA. Optimizing preparations of Co Fischer-Tropsch catalysts for stability against sintering. Appl Catal A: Gen 2020; 60225:117609.

[20] Wolf M, Fischer N, Claeys M. Water-induced deactivation of cobalt-based Fischer-Tropsch catalysts. Nat Catal 2020;3:962–5.

[21] Rodríguez-Gómez A, Platero F, Caballero A, Colón G. Improving the direct synthesis of hydrogen peroxide from hydrogen and oxygen over Au-Pd/SBA-15 catalysts by selective functionalization. Mol Catal 2018;445:142–51.

[22] Deng S, Chen N, Deng D, Li Y, Xing X, Wang Y. Meso- and macroporous coral-like Co3O4 for VOCs gas sensor. Ceram Int 2015;41:11004–12.

[23] Nakate UT, Bhuyan P, Yu YT, Park S. Synthesis and characterizations of highly responsive H2S sensor using p-type Co3O4 nanoparticles/nanorods mixed nanostructures. Int J Hydrog Ener 2022;47:8145–54.

[24] Swamy V, Kuznetsov A, Dubrovinsky LS, Caruso RA, Shchukin DG, Muddle BC. Finite-size and pressure effects on the Raman spectrum of nanocrystalline anatase TiO2. Phys Rev B 2005;71:184302.

[25] Choi HC, Jung YM, Kim SB. Characterization of Raman Spectra of size-selected TiO2 nanoparticles by two-dimensional correlation Spectroscopy. Bull Korean Chem Soc 2004;25:426–8.

[26] Khatun N, Rini EG, Shirage P, Rajput P, Jha SN, Sen S. Effect of lattice distortion on bandgap decrement due to vanadium substitution in TiO2 nanoparticles. Mater Sci Semicond Process 2016;50:7–13.

[27] Liu Z, Chen W-F, Zhang X, Zhang Ji, Koshy P, Sorrell CC. Structural and Microstructural Effects of Mo^{3+}/Mo^{5+} Codoping on Properties and Photocatalytic Performance of Nanostructured TiO2 Thin Films. J Phys Chem C 2019;123(18): 11781–90.

[28] Ma HL, Yang JY, Dai Y, Zhang YB, Lu B, Ma GH. Raman study of phase transformation of TiO2 rutile single crystal irradiated by infrared femtosecond laser. Appl Surf Sci 2007;253:7497–500.

[29] Zhu W, Chen X, Jin J, Di X, Liang C, Liu Z. Insight into catalytic properties of Co3O4-CeO2 binary oxides for propane total oxidation. Chin J Catal 2020;41(4): 679–90.

[30] Colón G, Hidalgo MC, Munuera G, Ferino I, Cutrufello MG, Navío JA. Structural and surface approach to the enhanced photocatalytic activity of sulfated TiO2 photocatalyst. Appl Catal B: Environ 2006;63:45–59.

[31] Li Y, Qiu W, Qin F, Fang H, Hadjiev VG, Litvinov D, et al. Identification of Cobalt Oxides with Raman Scattering and Fourier Transform Infrared Spectroscopy. J Phys Chem C 2016;120:4511–6.

[32] Kusiak-Nejman E, Sienkiewicz A, Wanag A, Rokicka-Konieczna P, Morawski AW. The Role of Adsorption in the Photocatalytic Decomposition of Dyes on APTES-Modified TiO2 Nanomaterials. Catalysts 2021;11:172.

[33] Rabee AIM, Gaid CBA, Mekhemer GAH, Zaki MI. Combined TPR, XRD, and FTIR studies on the reduction behavior of Co3O4. Mater Chem Phys 2022;289:126367.

[34] Li X, Nisa MU, Chen Y, Li Z. Co-Based Catalysts Supported on Silica and Carbon Materials: Effect of Support Property on Cobalt Species and Fischer-Tropsch Synthesis Performance. Ind Eng Chem Res 2019;58:3459–67.

[35] Kamath G, Badoga S, Shakouri M, Hu Y, Dalai AK. Influence of calcination on physico-chemical properties and Ficher-Tropsch activity of titanosilicate supported cobalt catalysts with different pore sizes. Appl Catal A: Gen 2020;598:117563.

[36] Eschemann TO, Bitter JH, de Jong KP. Effects of loading and synthesis method of titania-supported cobalt catalysts for Fischer-Tropsch synthesis. Catal Today 2014; 228:89–95.

[37] Jia C-J, Schwickardi M, Weidenthaler C, Schmidt W, Korhonen S, Weckhuysen BM, et al. Co3O4–SiO2 Nanocomposite: A Very Active Catalyst for CO Oxidation with Unusual Catalytic Behavior. J Am Chem Soc 2011;133(29):11279–88.

[38] Todorova S, Naydenov A, Kolev H, Holgado JP, Ivanov G, Kadinov G, et al. Mechanism of complete n-hexane oxidation on silica supported cobalt and manganese catalysts. Appl Catal A: Gen 2012;413–414:43–51.

[39] Zhong L, Kropp T, Baaziz W, Ersen O, Teschner D, Schlögl R, et al. Correlation Between Reactivity and Oxidation State of Cobalt Oxide Catalysts for CO Preferential Oxidation. ACS Catal 2019;9:8325–36.

[40] Echeverria E, Kaphle A, Austin A, Bastatas L, Hari P, Mcllroy D. Evolution of the Stoichiometry and Electronic Structure of Cobalt Oxide in Thermally Treated Co-Doped ZnO Nanorods for Solar Cells. ACS Appl Nano Mater 2019;2:4113–20.

[41] Huck-Iriart C, Soler L, Casanovas A, Marini C, Prat J, Llorca J, et al. Unraveling the chemical state of Cobalt in Co-based catalysts during Ethanol Steam Reforming: An in-situ study by Near Ambient Pressure XPS and XANES. ACS Catal 2018;8: 9625–36.

[42] Bertella F, Concepción P, Martínez A. TiO2 polymorph dependent SMSI effect in Co-Ru/TiO2 catalysts and its relevance to Fischer-Tropsch synthesis. Catal Today 2017;289:181–91.

[43] Borg Ø, Dietzel PDC, Spjelkavik AI, Tveten EZ, Walmsley JC, Diplas S, et al. Fischer-Tropsch synthesis: Cobalt particle size and support effects on intrinsic activity and product distribution. J Catal 2008;259:161–4.

[44] Krishnamoorthy S, Li A, Iglesia E. Patways for CO2 formation and conversion during Fischer-Tropsch synthesis on iron-based catalysts. Catal Lett 2002;80: 77–86.

[45] Jiang F, Zhang M, Liu B, Xua Y, Liu X. Insights into the influence of support and potassium or sulfur promoter on iron-based Fischer-Tropsch synthesis: understanding the control of catalytic activity, selectivity to lower olefins, and catalyst deactivation, Catal. Sci Technol 2017;7:1245–65.

[46] Tavasoli A, Sadaghiani K, Nakhaeipour A, Ahangari M. Cobalt Loading Effects on the Structure and Activity for Fischer-Tropsch and Water-Gas Shift Reactions of Co/Al2O3 Catalysts. Iran J Chem Chem Eng 2007;26:9–16.

[47] Scalbert J, Clémençon I, Lecour P, Braconnier L, Diehl F, Legens C. Simultaneous investigation of the structure and surface of a Co/alumina catalyst during Fischer-

Tropsch synthesis: discrimination of various phenomena with beneficial or disadvantageous impact on activity, Catal. Sci Technol 2015;5:4193–201.

[48] Rodrigues A, Tatibouët JM, Fourré E. Operando DRIFT Spectroscopy Characterization of Intermediate Species on Catalysts Surface in VOC Removal from Air by Non-thermal Plasma Assisted Catalysis. Plasma Chem Plasma Process 2016;36:901–15.

[49] Sanchez-Escribano V, Larrubia Vargas MA, Finocchio E, Busca G. On the mechanisms and the selectivity determining steps in syngas conversion over supported metal catalysts: An IR study. Appl Catal, A 2007;316:68–74.

[50] Meunier FC. The design and testing of kinetically-appropriate operando spectroscopic cells for investigating heterogeneous catalytic reactions. Chem Soc Rev 2010;39:4602–14.

[51] Gonugunta P, Dugulan AI, Bezemer GL, Brück E. Role of surface carboxylate deposition on the deactivation of cobalt on titania Fischer-Tropsch catalysts. Catal Today 2021;369:144–9.

[52] Schweicher J, Bundhoo A, Frennet A, Kruse N, Daly H, Meunier FC. DRIFTS/MS Studies during Chemical Transients and SSITKA of the CO/H_2 Reaction over Co-MgO Catalysts. J Phys Chem C 2010;114:2248–55.

[53] Lustemberg PG, Bosco MV, Bonivardi A, Busnengo HF, Ganduglia-Pirovano MV. Insights into the nature of formate species in the decomposition and reaction of methanol over cerium oxide surfaces: A combined infrared spectroscopy and density functional theory study. J Phys Chem C 2015;119:21452–64.

[54] Singh JA, Yang N, Liu X, Tsai C, Stone KH, Johnson B, et al. Understanding the Active Sites of CO Hydrogenation on Pt–Co Catalysts Prepared Using Atomic Layer Deposition. J Phys Chem C 2018;122:2184–94.

[55] Koley P, Shit SC, Sabri YM, Rao BS, Nakka L, Tardio J, et al. Looking into More Eyes Combining In Situ Spectroscopy in Catalytic Biofuel Upgradation with Composition-Graded Ag−Co Core−Shell Nanoalloys. ACS Sustainable Chem Eng 2021;9:3750–67.

[56] Jansson J, Palmqvist AE, Fridell E, Skoglundh M, Österlund L, Thormählen P, et al. On the Catalytic Activity of Co_3O_4 in Low-Temperature CO Oxidation. J Catal 2002;211:387–97.

[57] Cats KH, Andrews JC, Stéphan O, March K, Karunakaran C, Meirer F, et al. Active phase distribution changes within a catalyst particle during Fischer-Tropsch synthesis as revealed by multi-scale microscopy, Catal. Sci Technol 2016;6: 4438–49.

[58] Gonzalez-DelaCruz VM, Holgado JP, Pereñíguez R, Caballero A. Morphology changes induced by strong metal–support interaction on a Ni–ceria catalytic system. J Catal 2008;257:307–14.

[59] A. Caballero, J.P. Holgado, V.M. Gonzalez-delaCruz, S.E. Habas T. Herranz, M. Salmeron. In situ spectroscopic detection of SMSI effect in a Ni/CeO_2 system: Hydrogen-induced burial and dig out of metallic nickel. Chem. Commun. 46, (2010), pp. 1097–1099.